Electronic structure of quasicrystalline surfaces: Effects of surface preparation and bulk structure

V. Fournée,[1] P. J. Pinhero,[1] J. W. Anderegg,[1] T. A. Lograsso,[1,2] A. R. Ross,[1] P. C. Canfield,[1,3] I. R. Fisher,[1,3] and P. A. Thiel,[1,4]

[1]*Ames Laboratory, Iowa State University, Ames, Iowa 50011*

[2]*Department of Materials Science and Engineering, Iowa State University, Ames, Iowa 50011*

[3]*Department of Physics and Astronomy, Iowa State University, Ames, Iowa 50011*

[4]*Department of Chemistry, Iowa State University, Ames, Iowa 50011*

(Received 14 April 2000)

We elucidate the nature of the surface electronic properties of quasicrystalline Al-Pd-Mn. We do this by using photoelectron and Auger electron spectroscopies, and by making a variety of comparisons—across types of bulk samples, and across methods of surface preparation. The main conclusions are these: (i) The narrow Mn $2p_{3/2}$ core-level line observed in the icosahedral phase is a fingerprint of a suppression in the density of states (a pseudogap) at the Fermi level and is not unique to the quasicrystalline phase. It is also independent of the symmetry of the quasicrystalline surface. The Auger line shape is also affected and may be used as a fingerprint of a pseudogap. (ii) A similarly narrow Fe $2p_{3/2}$ core-level line characterizes the icosahedral Al-Cu-Fe quasicrystal, consistent with the expectation that the electronic structure is of general importance in the stabilization of icosahedral phases. (iii) In icosahedral Al-Pd-Mn, the pseudogap of the bulk is not retained up to the surface immediately after fracture, but can be restored by annealing, or by sputter annealing to sufficiently high temperatures. Assuming that the pseudogap reflects an electronic stabilization of the atomic structure, these results suggest that the heat-treated surfaces are more stable than the surface obtained by fracturing at room temperature.

I. INTRODUCTION

Quasicrystals, discovered in 1982 by D. Shechtman,[1] possess a remarkable atomic structure—remarkable in the sense that the atomic positions are well ordered, yet aperiodic. There has been a growing appreciation within the scientific community that this unique atomic structure is associated with an unusual combination of electronic, physical, and mechanical properties.[2] However, the nature of the relationship between quasiperiodic structure and macroscopic properties remains today a subject of intense discussion and research.

Among the most intriguing properties are the surface properties. These include low coefficients of friction, oxidation-resistance, and reduced adhesion.[3–5] It is extremely important to understand how and why these properties arise. One central issue is the electronic character of the surface. For instance, is it similar to that of the bulk or not? And how does the answer to this question depend upon conditions of surface preparation? Understanding the electronic character of the intrinsic surface is basic to understanding the nature of chemical reactions with its environment, such as wetting by liquids.

It is well known that the method of surface preparation can have a profound effect on surface topography of quasicrystals, at the nanometer scale. Specifically, preparation of a clean surface by sputtering and annealing in ultrahigh vacuum can yield a surface with a terrace-step topography,[6–8] whereas preparation by fracture (also in ultrahigh vacuum) exposes a much rougher surface, dominated by a cluster structure.[9,10] As yet, it has not been determined whether these differences in topography are accompanied by differences in electronic structure. One of the goals of this paper is to explore this issue.

Electronic surface structure is probed primarily by photoemission techniques, which are commonly used in two broad spectral regions: the valence band or the core levels. The first of these, the valence band, is important to quasicrystals because it contains the pseudogap—the reduction in the density of states at E_F—which is characteristic of the bulk. For the valence band, Stadnik *et al.* used ultrahigh-energy-resolution ultraviolet spectroscopy and observed a clear Fermi edge for the surface of the icosahedral (*i*-) phase of Al-Pd-Mn, with a spectral intensity only weakly decreasing towards the Fermi level, E_F.[11,12] For the same type of quasicrystal, however, Wu *et al.* observed a distinct pseudogap feature, with a density of states (DOS) decreasing as a power law near E_F.[13] In this latter case, the quasicrystalline ordering of the surface could be checked by observing the low-energy electron-diffraction (LEED) pattern. While the differences between the two sets of results were attributed to differences in sample temperature,[11,12] significant differences in preparation history also existed. This approach has also been used recently by Naumovic *et al.*[14] who concluded that a surface prepared in the manner of Wu *et al.* indeed displays a suppressed density of states at E_F, compatible with a pseudogap.

The second route to determining electronic properties with photoemission is through core level line-shape analysis of x-ray photoelectron spectra (XPS). It is well known that core level lines in x-ray excited photoemission spectra of metallic compounds show an asymmetric tail.[15] This is due to the screening response of the valence electrons to the cre-

ation of the core hole. The asymmetry of the line shape results from intrinsic energy losses through the excitation of electron-hole pairs that are created simultaneously with the core hole.[16] The probability of these processes decreases rapidly with the electron-hole pair energy. Therefore the main contribution comes from low-energy electron excitations across the Fermi level. This implies that the asymmetry of the XPS core level lines depends on the local DOS *at the Fermi level* $\rho(E_F)$.[17] This effect can be used as a tool to probe the valence electrons in metallic compounds.

C. J. Jenks *et al.*[18] (hereafter referred as CJJ) first reported such a line-shape analysis of a fivefold surface of a quasicrystalline alloy, $Al_{70}Pd_{21}Mn_9$, prepared by sputtering and annealing at temperatures higher than 700 K. The two main features observed, relative to nonquasicrystalline surfaces, are (i) a large shift of the Pd $3d$ lines toward high binding energies, and (ii) a narrowing of the Mn $2p_{3/2}$ line. These observations have been confirmed.[19] Using the Doniach-Sunjic XPS line shape to fit the experimental data, CJJ found that the narrowing of the Mn $2p_{3/2}$ line is due to a decrease of both the asymmetry parameter and the core-level width, indicative of a combination of electronic effects near the Fermi edge. The narrowing of the Mn $2p_{3/2}$ line was postulated to be the fingerprint of a well ordered quasicrystalline surface.[18]

In the present work, extensive use of the Doniach-Sunjic line-shape analysis is made to determine electronic characteristics of the clean surfaces of the *i*-Al-Pd-Mn quasicrystal and their dependence upon the conditions of preparation. We compare surfaces prepared by fracturing (followed in some cases by annealing), and by sputtering and annealing at various temperatures. Sputtering changes the composition; annealing allows structural rearrangements. More specifically, sputtering followed by annealing to temperatures below about 700 K produces a crystalline phase, a $B2$ (CsCl-like) structure as revealed by several techniques,[14,20–22] including LEED structural analysis.[23] Annealing to higher temperatures allows long-range bulk-surface equilibration, and a surface that displays characteristics consistent with a bulklike termination of the quasicrystalline structure.[20,24] Hence one can form crystalline or quasicrystalline surfaces on a single sample by controlling the temperature program after sputtering. We exploit this capability in the present work.

Comparisons with surfaces of *bulk* crystalline phases are also revealing, and interesting results for the ξ'-Al-Pd-Mn approximant as well as for the cubic $Al_{60}Pd_{25}Mn_{15}$ and the orthorhombic o-Al_6Mn crystals are presented in this paper. The fivefold surface of the icosahedral *i*-AlCuFe phase has also been investigated. Hence this paper analyzes a database spanning several crystalline and quasicrystalline bulk structures, and two main methods of sample preparation (fracturing vs sputter annealing). Sections III A–F serve to establish this database, each section being devoted to a different type of sample.

Furthermore, by varying the mean escape depth of the photoelectrons, we are able to probe the density of states at the Fermi level as a function of distance from the surface. The Doniach-Sunjic line-shape analysis reveals that the pseudogap of the bulk is not retained up to the nascent fractured surface, whereas it is retained when the surface has been fractured and annealed, or sputtered and annealed. This surprising result will be presented in Sec. III G.

Finally, the Mn-*LMM* Auger lines have also been investigated. These transitions involve the Mn $3d$ states lying close to the Fermi level. Their line shapes provide valuable information because they are closely related to that of the Mn $2p_{3/2}$ XPS line and depend on the local electronic structure around Mn atoms. This is a different approach to probing the electronic structure of quasicrystals, and is presented in Sec. III H. A general discussion follows in Sec. IV.

II. EXPERIMENTAL DETAILS

A. Sample preparation

For the fracture experiments, two single grain quasicrystals of *i*-Al-Pd-Mn were grown by the Bridgman technique.[25] One was oriented along a fivefold axis, using back-reflection Laue analysis, with an accuracy of $\pm 2°$. A higher accuracy is not useful as the fracture process introduces a larger uncertainty on the final orientation of the surface. The bulk composition, as determined by inductively coupled plasma atomic emission spectroscopy (ICP-AES), is $Al_{70.5\pm0.7}Pd_{20.5\pm0.1}Mn_{9\pm0.1}$. (The error bars reflect precision, not accuracy.) The other single grain was oriented parallel to a threefold axis and has a nominal composition (i.e., the initial liquid composition used in growth) of $Al_{70}Pd_{21.5}Mn_{8.5}$. Two rod-shaped samples ($2.5\times2.5\times18\ mm^3$) were cut using an electronic discharge machine (EDM) from each single grain. The phase purity was checked by scanning Auger microscopy (SAM) and scanning electron microscopy (SEM). Some Mn rich second phase could be detected at the bottom of the rods. By mapping the samples from bottom to top using SAM/SEM, we were able to fracture the samples in the single-phase region.

Some experiments were performed on surfaces that were mechanically polished, then sputter annealed in UHV. This was true for a fivefold surface of *i*-Al-Pd-Mn grown by the Bridgman technique, the same quasicrystalline sample as used in the previous photoemission work of CJJ.[18] This was also true for a fivefold surface of an *i*-AlCuFe single grain, grown by isothermal, liquid-assisted grain ripening.[26,27] The bulk composition, as determined by ICP-AES is $Al_{63.4\pm0.4}Cu_{24\pm0.9}Fe_{12.6\pm0.5}$. More details about sample preparation have been given elsewhere.[28]

The ξ'-AlPdMn approximant is an orthorhombic crystal with a large unit cell.[29] The sample was produced by the flux growth technique[30] from a liquid of composition $Al_{80.5}Pd_{17.25}Mn_{2.25}$.[31] A sample with an approximate size of $2\times2\times12\ mm^3$, oriented along the pseudotenfold axis was used for XPS experiments.

The cubic alloy was grown from a melt of starting composition $Al_{60}Pd_{25}Mn_{15}$. It is a single crystal with the CsCl-like ($B2$) structure. The lattice constant, determined by x-ray diffraction, is 3.02 Å. The sample is roughly $15\times6\times1\ mm^3$ in size. Its surface happens to be oriented 9.5° from the (111), 29° from the (110) and 48° from the (100).

The orthorhombic alloy, o-Al_6Mn, was drop cast from a melt of composition $Al_{85.8}Mn_{14.2}$. The sample was then heated at 900 K for 7 days. It is multigrain sample. The space group is *Cmcm*, and the lattice parameters are $a=7.555$ Å, $b=6.499$ Å, $c=8.872$ Å.[32] X-ray diffraction

showed the presence of a small amount of pure Al. Two rodlike samples were cut by EDM for fracture experiments.

The cubic AlPdMn crystal and the *i*-AlCuFe quasicrystal were not available in a form suitable for *in situ* fracture. For these samples, a clean surface was obtained in UHV only by cycles of ion sputtering (4 keV of Ar^+) and annealing at temperatures up to 920 K for about 15 min, until no traces of oxygen or carbon could be detected. As noted above, this method was also applied to one fivefold surface of *i*-Al-Pd-Mn that had been oriented and polished mechanically.

In all other cases, we proceeded as follows. The sample was introduced into the preparation chamber where it was outgassed at temperatures ranging from 570 to 870 K for 30 min. Then the sample was cooled to either room temperature or liquid-nitrogen temperature, and fractured. We call this the nascent fractured surface, to distinguish it from the fractured surface which has been annealed above room temperature. It takes about 7 min to transfer the fractured surface into the XPS chamber. The base pressure is maintained below 4×10^{-10} torr during the whole experiment. We could not detect the presence of oxygen or other impurities on the fractured surface, so long as the temperature was held below the initial outgassing temperature.

B. XPS and XAES parameters

The photoelectron spectra were acquired using a Perkin-Elmer Multitechnique Chamber, Model 5500, fitted with an Omni Focus III lens system, and monitored with PHI-ACCESS software. The x-ray source is a monochromatized Al $K\alpha$ radiation. The takeoff angle was set to 45°, unless we specify otherwise. Under these conditions, XPS and x-ray induced Auger electron spectroscopy (XAES) measurements provide a depth-weighted average over the top 50–100 Å of material, which we shall refer to as the surface/near-surface region. Energy calibration of the spectrometer was achieved using the Au $4f_{7/2}$ (84.0 eV) and Cu $2p_{3/2}$ (932.7 eV) lines. The resolution was 0.65 eV for a 29.5-eV pass energy. XAES was performed under the same conditions, with takeoff angle set to 45°. The XPS valence bands presented here are corrected for secondary-electron background.

C. Fitting procedure

For a metal, the response of the electron gas to the creation of the core hole is taken into account in the line-shape formula derived by Doniach and Sunjic:[33]

$$Y(E)=\frac{\Gamma(1-\alpha)}{[(E-E_0)^2+\gamma^2]^{(1-\alpha)/2}}\cos\left[\frac{\pi\alpha}{2}+(1-\alpha)\tan^{-1}\left(\frac{E-E_0}{\gamma}\right)\right],$$

where Y is the intensity, Γ is the gamma function, E_0 is the binding energy, γ is the lifetime broadening of the core level, and α is the asymmetry parameter. This function reduces to a Lorentzian with a full width at half maximum (FWHM) equal to 2γ for $\alpha=0$. A higher value of α means a higher $\rho(E_F)$. Variations on this function have been worked out for cases in which the DOS near E_F is not constant on the energy scale of the linewidth.[34] A Gaussian experimental function convoluted with the Doniach-Sunjic function is used to fit our data. The width of the experimental function is obtained by fitting the Gaussian convoluted with a Fermi-Dirac distribution function to the measured Fermi edge of Ag. The secondary electron background is accounted for by a third-order polynomial. The line shape and background are fitted to the spectra simultaneously.[35] The α parameter is constrained to be the same for the core levels of the same elements. The free parameters (α, γ, E_0, peak intensity and the coefficients of the background) are adjusted by minimizing χ^2. The fitting is carried out using Marquardt's algorithm for unconstrained minimization of a nonlinear function. The relevance of the model and the quality of the fit can be judged by the residual. The values of the parameters reported in the tables and text are the average values obtained from all the photoelectron spectra acquired with the same experimental conditions for each sample.

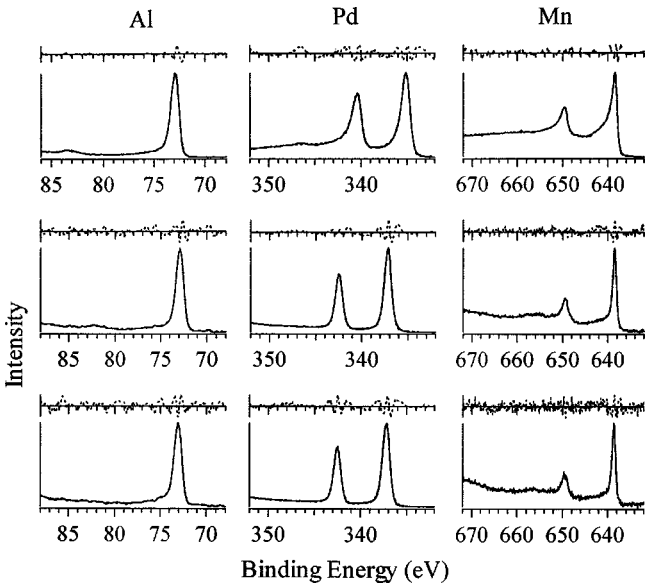

FIG. 1. Doniach-Sunjic fit to the experimental spectra for Al, Pd, and Mn. Solid lines represent the experimental spectra, bottom dashed lines are the fits, and top dashed lines shows the residuals. The vertical scales for the residuals is expanded by 5 relative to the vertical scale of the experimental spectra. The top row shows results for the pure metals. The second row shows results for the fractured fivefold surface of the quasicrystal. The bottom row shows results for the fivefold surface prepared by sputtering and annealing at 870 K.

III. RESULTS AND DISCUSSION

A. Fivefold surface of icosahedral AlPdMn: Surface and near-surface region combined

The photoelectron spectra of the fractured fivefold surface are displayed in Fig. 1. They are compared to those obtained for the sputter-annealed surface at 870 K. (This annealing temperature yields a surface whose LEED pattern, and other characteristics, are consistent with surface quasicrystallinity.[6–8,13,24,36,37] Spectra for the pure elements Al, Pd, and Mn are also presented. The parameters obtained from the fits are given in Table I. For Al, we give only the

TABLE I. Fitting parameters corresponding to the data of Fig. 1. The standard deviation for the α values given by the fitting program are: $+/-0.005$ for Mn after fracture; $+/-0.007$ for Mn after sputter annealing; $+/-0.003$ for Pd after fracture; $+/-0.003$ for Pd after sputter annealing.

	Al $2p$			Pd $3d$					Mn $2p$			
				3/2		5/2			1/2		3/2	
Sample	E_B	W	α	E_B	2γ	E_B	2γ	α	E_B	2γ	E_B	2γ
Pure metal annealed at $T>800$ K	72.8	0.96	0.21	340.3	0.49	335.0	0.35	0.46	649.3	1.02	638.3	0.38
5f-AlPdMn just after fracture	72.9	1.06	0.05	342.5	0.35	337.2	0.35	0.21	649.3	1.07	638.4	0.27
5f-AlPdMn sputter annealed at 870 K	73.0	1.08	0.05	342.5	0.37	337.2	0.37	0.18	649.3	1.15	638.4	0.29

value of the binding energy (E_B) and the full width at half maximum (FWHM) because the $2p_{1/2}$ and $2p_{3/2}$ components are unresolved.

The spectra of the fivefold surface prepared by fracturing or by sputter annealing look very similar and core-level binding energies agree within ± 0.1 eV, which is the experimental accuracy. Results for the sputter-annealed surface reproduce those reported previously by CJJ.[18] There are three general trends.

First, the binding energy of the Pd $3d$ levels is 2.2 eV higher in the quasicrystal than in pure Pd. A shift of 0.2 eV is also found for Al $2p$ core levels whereas no significant shift is observed for Mn $2p$ levels. This is independent of surface preparation for the quasicrystal, within the methods spanned by Fig. 1. The large chemical shift of the Pd core levels is consistent with other values observed in different Al-Pd alloys.[18]

Second, the Mn $2p_{3/2}$ line is very narrow for the fractured surface and the sputter-annealed one, relative to metallic Mn. This is due to a combination of two effects. First, the asymmetric tail toward higher binding energies is suppressed; as can be seen from the small α values derived from the fits. Second, the intrinsic width of the $2p_{3/2}$ core level, reflected in the 2γ values, is somewhat lower for the quasicrystal than for pure Mn. For Mn, it was observed previously that the narrowing of the Mn $2p_{3/2}$ line is very sensitive to the details of the structural and chemical environment. For example, the sputtered surface, before annealing, does not show this narrowing of the Mn $2p_{3/2}$ line, because the surface is not quasicrystalline. The local DOS at E_F around the Mn atoms, which strongly depends on the position of the Mn $3d$ band relative to E_F, can be modified with structural changes, with corresponding effect on the line shape of Mn $2p_{3/2}$. The fact that no differences are observed between the fractured and the sputter-annealed surfaces in Fig. 1/Table I suggests that the atomic environments within the top 50–100 Å are very similar for the two types of surface preparation.

Note that the values of 2γ are much different than those reported by CJJ,[18] due to an error in the previous line-shape analysis. The trends in comparisons between different types of surfaces, however, remain unchanged.

Third, the values of α for the Pd peaks are also very small in the quasicrystal as compared to the pure elements. This is due to the fact that the Pd $4d$ band is shifted in the alloy by about 2 eV toward higher binding energies [to about 4.2 eV below E_F (Refs. 13 and 38)] relative to Pd metal. The local DOS at E_F around Pd atoms is therefore suppressed, which is consistent with a low value of α.

These data show that the electronic structure of the fivefold surface, averaged over the combined surface and near-surface region, does not depend upon whether the quasicrystalline surface is prepared by fracture or by sputter annealing.

B. Fivefold surface of icosahedral AlCuFe: Surface and near-surface region combined

The AlCuFe and AlPdMn icosahedral phases have similar valence band structure: the Cu $3d$ and Fe $3d$ bands behave like the Pd $4d$ and Mn $3d$ bands, respectively. The photoelectron spectra of Fe $2p$ core levels, obtained for the fivefold surface of *i*-AlCuFe prepared by sputter annealing, and for a (110) face of pure Fe, are displayed in Fig. 2. The

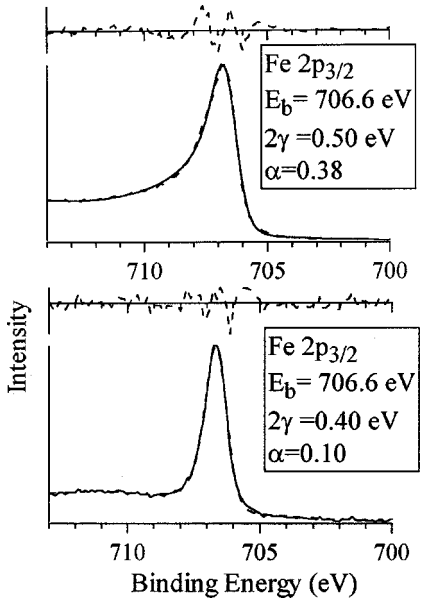

FIG. 2. Doniach-Sunjic fit to the Fe $2p_{3/2}$ in pure Fe (left) and in the ι-AlCuFe quasicrystal. Solid lines represent the experimental spectra, bottom dashed lines are the fits, and top dashed lines shows the residuals. The vertical scales for the residuals is expanded by 5 relative to the vertical scale of the experimental spectra.

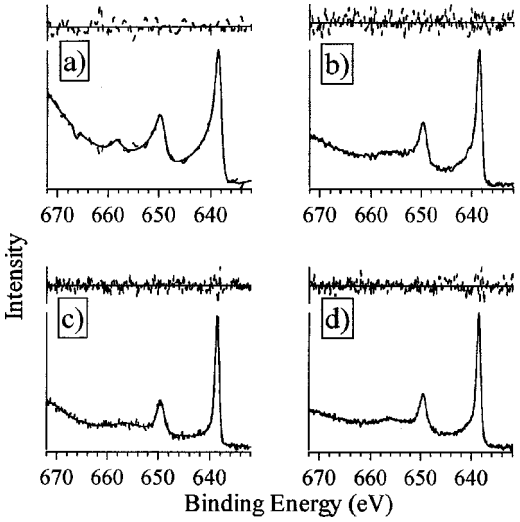

FIG. 3. Doniach-Sunjic fits of the Mn $2p$ lines on the threefold *i*-AlPdMn surface. (a) After etching and annealed at 540 K. (b) After etching and annealed at 720 K. (c) Annealed at 770 K. (d) Just after fracture.

parameters obtained from the fits are reported in the figure. Like the Mn line in the AlPdMn system, a narrowing of the Fe $2p_{3/2}$ line is observed in *i*-AlCuFe, which is due to a decrease of both the asymmetry parameter and the core-level width. Following the same method of preparation of the surface, it has been demonstrated that this icosahedral phase exhibits a characteristic fivefold LEED pattern.[39] These results show that at least two different icosahedral alloys exhibit the narrowing of the XPS line associated with the minority metal component.

C. Threefold surface of icosahedral AlPdMn: Surface and near-surface region combined

We mentioned above that the shape of the Mn $2p$ core level is very sensitive to the details of the structural and chemical environment. This was based upon comparisons revolving around the fivefold[18] and twofold surfaces of *i*-Al-Pd-Mn.[40] Here, we expand that comparison to include the threefold surface.

Figure 3 shows the Doniach-Sunjic fits of the Mn $2p$ lines of the threefold surface of the icosahedral phase obtained after different treatments. Figure 4 shows the corresponding valence-band (VB) spectra, recorded at a higher resolution: 0.37 eV for a 5.85-eV energy pass. The strongest peak in the VB photoemission spectra is located about 4.2 eV from E_F and is due to the Pd $4d$ states. Its position moves slightly toward higher binding energies, from 3.9 to 4.2 eV, when the sputtered surface is annealed from 540 to 770 K. Similarly, the Pd $3d$ core level binding energies shift by 0.3 eV, in going from 540 to 770 K, after sputtering. Fits of the Mn $2p$ core-level lines indicate a continuous narrowing upon annealing due to a decrease of both the asymmetry parameter and the core-level width. The first four rows of Table II give the fitting parameters. Once the sputtered surface is heated to sufficiently high temperature, the electronic structure, as observed by valence band and core-level photoemission spectra, is identical to that of the fractured surface.

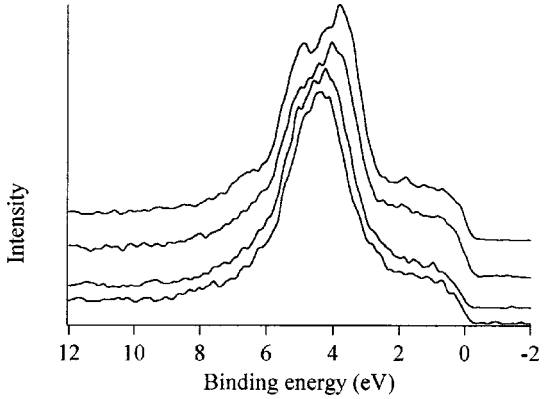

FIG. 4. Valence band of the fractured threefold *i*-AlPdMn surface after different treatment. From top to bottom: after sputter annealing at 540 K, after sputter annealing at 720 K, after annealing at 770 K, and just after fracture at room temperature.

The position of the Pd $4d$ band relative to E_F is determined by its interaction with the Al band, which is sensitive to the Pd-Al coordination number and bond length.[41] The shift of the Pd $4d$ band indicates a weaker interaction between Al and Pd atoms in the $B2$ overlayer than in the quasicrystalline surface.[20] The reduction of the asymmetry parameter of the Mn $2p$ core-level lines indicates a reduction of the local DOS at the Fermi level around Mn atoms upon annealing through this transition. At the same time, the slope of the VB photoemission spectra in the region near E_F is reduced. After sputtering and annealing at low temperature, the slope of the VB around E_F is the same as that observed for Ag, and therefore exhibits a clear Fermi edge. Once the same sample has been fully annealed at sufficiently high temperature, the slope of the VB edge is reduced. The VB spectra are all recorded at room temperature with identical spectrometer settings, which means that the thermal and experimental broadening are the same for all spectra. The VB spectra alone would not allow us to infer the presence of a pseudogap in the DOS, due to the limited resolution of the XPS measurement, but are compatible with the more conclusive core-level line-shape analysis.

These XPS results show that the structural modifications observed by LEED on the sputtered surface upon annealing, from a cubic $B2$ structure below 700 K to a quasicrystalline

TABLE II. Parameters of the fits to the data of Fig. 4.

		Mn $2p$			
				3/2	
Sample	α	E_B	2γ	E_B	2γ
$3f$-AlPdMn sputter annealed at 540 K	0.43	649.3	1.5	638.2	0.51
$3f$-AlPdMn sputter annealed at 720 K	0.31	649.3	1.4	638.3	0.39
$3f$-AlPdMn annealed at 770 K	0.22	649.3	1.0	638.4	0.31
$3f$-AlPdMn after cleavage	0.22	649.3	1.2	638.4	0.30
Cubic alloy annealed at 870 K	0.43	649.3	1.49	638.2	0.53

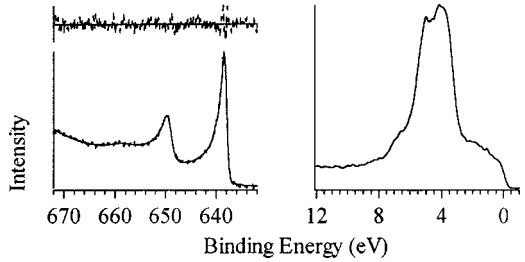

FIG. 5. Mn $2p$ core-level spectra (left) and valence band (right) for the cubic AlPdMn alloy.

structure for $T \approx 770$ K, are accompanied by the opening of a pseudogap at E_F. Naumovic *et al.* have reached a similar conclusion using the same type of VB measurement on i-AlPdMn.[14]

The opening of the pseudogap upon annealing is in agreement with the experimental fact that the quasicrystalline surface and near-surface structure is thermodynamically stable relative to cubic overlayers that form at lower annealing temperatures.[20] It is well known that the presence of a pseudogap at E_F reduces the band energy contributing to the total energy, providing a better stability to the system.[42]

The similarity of the data for the threefold, twofold,[40] and fivefold[18] surfaces of this quasicrystal indicates that surface symmetry plays no role in the average electronic properties as probed with our techniques.

D. Cubic phase of AlPdMn: Surface and near-surface region combined

We turn now to the surface of the *bulk* cubic ($B2$) sample. Interestingly enough, the photoelectron spectra of the cubic AlPdMn crystal are very similar to the those of the surface of the icosahedral phase when it is prepared by sputtering and annealing at temperatures below 700 K, as presented already in Sec. III C and Ref. 18.

Figure 5 shows the fits to the experimental core-level lines of Pd and Mn, as well as the valence band of the crystal. Parameters of the fits are given in the last row of Table II. As reported earlier by CJJ,[18] the value of α for the Pd peaks is quite robust and does not vary significantly in the alloys considered. This is due to the fact that the Pd $4d$ band lies well below E_F in the alloys, implying a reduced $\rho(E_F)$ around Pd atoms and a smaller α as compared to pure Pd. The α value of Mn $2p$ is close to that of pure Mn and equals that of the low-temperature annealed threefold surface (see Table II), as do the binding energies and the intrinsic FWHM 2γ. The valence band of both surfaces also looks very similar. The main peak, attributed to the Pd $4d$ states, presents the same structures. The small structure located about 6.5 eV below E_F is also present. The DOS in the region near E_F of the cubic sample shows a sharp Fermi edge, almost as sharp as the Fermi edge of silver taken within the same experimental conditions. In conjunction with the large tail of the Mn $2p$ core-level lines, this shows that there is still a high density of Mn $3d$ states at the Fermi level. No pseudogap has appeared at E_F in this alloy.

The composition of the cubic alloy, measured by XPS, after sputtering and annealing at 870 K, is $Al_{57\pm2}Pd_{36\pm2}Mn_{7\pm2}$. The composition measured for the threefold i-AlPdMn surface after sputtering and annealing at 540 K is $Al_{59\pm2}Pd_{35\pm2}Mn_{6\pm2}$, which is quite close, and the structure of this surface as determined by LEED is also $B2$ (CsCl-like structure). Therefore it is not surprising to find similar electronic properties between the two surfaces.

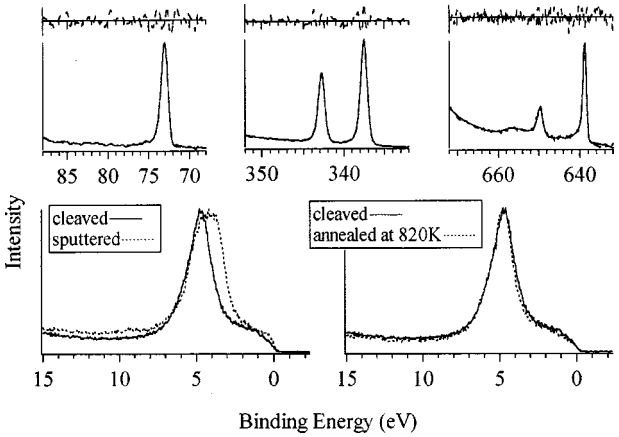

FIG. 6. Photoelectron spectra for the ξ'-AlPdMn approximant. The top row shows the Doniach-Sunjic fit to the experimental spectra for Al, Pd, and Mn core-level lines obtained on the fractured surface. Solid lines represent the experimental spectra, bottom dashed lines are the fits, and top dashed lines shows the residuals. The vertical scales for the residuals is expanded by 5 relative to the vertical scale of the experimental spectra. The bottom row compares the valence band for different states of that surface: after fracture, after etching, and after annealing at 820 K.

E. ξ'-AlPdMn approximant phase: Surface and near-surface regions combined

The composition after fracture given by XPS is $Al_{73\pm2}Pd_{22.5\pm2}Mn_{4.5\pm2}$. After annealing at 920 K, the Mn concentration decreases. Like the icosahedral phase, the sample undergoes a strong Pd enrichment (and Al depletion) upon ion bombardment at room temperature. After sputtering and annealing at 920 K, the composition measured at room temperature is $Al_{74.5}Pd_{24.5}Mn_1$.

The photoelectron spectra are displayed in Fig. 6, together with the Doniach-Sunjic fits and the residuals. The first row shows the Al $2p$, Pd $3d$, and Mn $2p$ core-level lines for the fractured surface. Parameters obtained from the fits are given in Table III, for the surface prepared either by fracturing or by sputtering and annealing. The second row compares the VB obtained just after fracture, after sputtering, and after annealing.

Relative to the icosahedral phase, no significant binding energy shifts are observed for the Al $2p$ and Mn $2p$ core levels. The shift of the Pd $3d$ core levels is higher in ξ' by 0.3 eV as compared to the quasicrystal. A narrow Mn $2p_{3/2}$ core-level line is also observed in this approximant. The values of the asymmetry parameter α are similar to those found for the quasicrystalline phase, both for Mn and Pd. The VB structure of the ξ'-AlPdMn approximant phase resembles that of the quasicrystalline phase. The main peak, which is due to Pd $4d$ states, broadens significantly upon sputtering and the VB in the region near E_F shows a sharp Fermi edge. Simultaneously, an asymmetric tail of the Mn $2p_{3/2}$ core-level line is observed. After annealing at 820 K, both the VB

TABLE III. Fitting parameters corresponding to the data of Fig. 6.

	Al $2p$			Pd $3d$					Mn $2p$			
				3/2		5/2			1/2		3/2	
Sample	E_B	W	α	E_B	2γ	E_B	2γ	α	E_B	2γ	E_B	2γ
ξ'-AlPdMn just after fracture	73.0	0.84	0.05	342.7	0.41	337.7	0.41	0.17	649.4	1.10	638.5	0.29
ξ'-AlPdMn sputter annealed at 920 K	73.1	0.97	0.05	342.8	0.42	337.5	0.43	0.13	649.4	1.20	638.6	0.31

and the core-level line recover the shape observed on the nascent fractured surface. These features indicate a rearrangement of the short and middle range atomic order upon annealing, which affects the electronic structure in a way similar to the quasicrystalline counterpart. That is, the DOS at E_F is reduced after annealing to high temperature, as evidenced by the narrow Mn $2p_{3/2}$ line and in agreement with the reduced slope of the VB edge. This is not unreasonable, as high-order approximant phases possess similar atomic order and physical properties often indistinguishable from their parent quasicrystal. This has been verified for various systems, such as AlCuFe (Ref. 43) or AlMgZn.[44]

This comparison shows that a narrow XPS Mn $2p_{3/2}$ core-level line should not be considered as the fingerprint of a quasicrystal, but only as an indication that a phase with a low DOS at E_F has formed. The existence of a pseudogap at E_F is a generic property of quasicrystals, but is not specific to them. In other words, a narrow XPS Mn $2p_{3/2}$ line can be considered a necessary, but not sufficient, condition for identifying the icosahedral phase in the Al-Pd-Mn system. (See Table IV.)

F. Case of a Hume-Rothery crystalline phase, Al_6Mn: Surface and near-surface regions combined

The orthorhombic phase o-Al_6Mn gives a further example of that. The Mn $2p_{3/2}$ core-level line also exhibits a reduced width, here again due to the decrease of both the core-level width 2γ and the asymmetry parameter α (Fig. 7). No significant difference could be observed between the two methods of preparation, fracturing or sputter annealing. The low α value indicates again a reduction of the local DOS $\rho(E_F)$ around the Mn atoms, as compared to pure Mn. The valence band has not been investigated, due to the presence of a small amount of pure Al in our sample that would contribute to the photoemission spectra. However, a band-

TABLE IV. Concentrations measured by XPS (in atomic percent). Since these values are obtained without calibration of sensitivity factors, the relative values should be considered rather than the absolute values. The number of measurements is given by n.

Condition and Sample	Al	Pd	Mn	n
5f-AlPdMn after fracture	68.3	19.3	12.4	9
5f-AlPdMn after annealing (550 °C)	68	21.5	9.5	5
5f-AlPdMn sputter annealed (550 °C)	68	25.2	6.7	4
3f-AlPdMn after fracture	67.4	21.3	11.2	14
3f-AlPdMn after annealing (550 °C)	68.8	23.9	7.3	4
3f-AlPdMn sputter-annealed (550 °C)	64.7	26.5	8.8	3
ξ'-AlPdMn after fracture	73	22.5	4.5	4
ξ'-AlPdMn after annealing (600 °C)	74.7	24.1	1.1	2
ξ'-AlPdMn sputter annealed (600 °C)	74.4	24.6	1.0	5
Al_6Mn after fracture	77.5		22.5	1
Al_6Mn after annealing (550 °C)	81		19	1
Al_6Mn sputter annealed (550 °C)	82.5		17.5	1

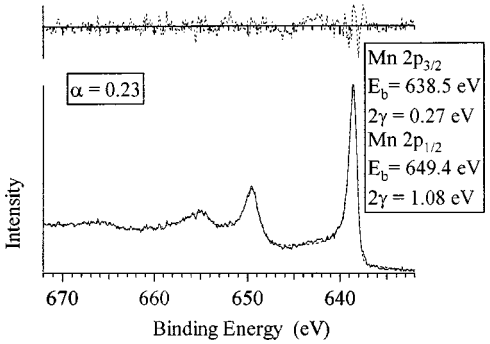

FIG. 7. Doniach-Sunjic fit to Mn $2p$ core-level line in Al_6Mn for the fractured surface. Solid line represent the experimental spectra, bottom dashed line is the fit, and top dashed line shows the residuals. The vertical scales for the residuals is expanded by 5 relative to the vertical scale of the experimental spectra.

structure calculation has been published for this alloy.[45] The main contribution to the total DOS in the region around the Fermi level is due to Mn $3d$ states, hybridized with Al states. In this Hume-Rothery alloy, the diffraction of the Fermi electrons by the Bragg planes as well as the coupling of the Al sp states with the Mn $3d$ states, strongly modifies the density of states and induces a deep pseudogap at E_F. This is in agreement with the low $\rho(E_F)$ around Mn atoms deduced from the photoelectron spectra (i.e., reduced density of Mn $3d$ states at E_F).

Two other broad peaks can be seen on the high binding energy side of the main peaks. They are located at 655.1 and 665.7 eV, i.e., 16.6 eV apart from Mn $2p_{3/2}$ and Mn $2p_{1/2}$, respectively. This energy-loss structure can be attributed to the excitation of a volume plasmon. Such structure can also be identified in the photoelectron spectra of the icosahedral phase, with a broader distribution and a much lower intensity, and an excitation energy of 17 eV. The existence of plasmons in quasicrystals have already been observed, mainly by electron energy-loss spectroscopy.[46] Energies of the plasmons and trends in the intensity and the line broadening agree well with published results. Such a line broadening is attributed to the fast decay of plasmons into interband transitions, involving mainly the transition-metal d states. The differences in intensity and width of the plasmon satellite, between the o-Al_6Mn crystal and the icosahedral AlPdMn phase, have been ascribed to either compositional changes or to the peculiar band structure of the icosahedral quasicrystals.[46]

G. Increasing the surface sensitivity of x-ray photoelectrons

The photoelectron spectra presented above were recorded with a takeoff angle set to 45°. The mean escape depth of the photoelectrons depends on their kinetic energy and on the takeoff angle. The energy of our x-ray source being fixed (Al $K\alpha = 1486.6$ eV), we cannot change the kinetic energy of the photoelectrons but we can vary the takeoff angle to become more surface sensitive. The elastic mean-free path (λ_m) of the photoelectrons in the quasicrystal can be estimated by using a modified form of the Bethe equation.[47] The calculation of λ_m requires knowledge of the plasmon energy and the density of the material. We use values published in the literature: 0.064 at./Å^3 for the atomic density[48] and 16.4 eV for the plasmon energy.[46] The calculated λ_m are then 33, 23, and 18 Å for Al $2p$, Pd $3d$, and Mn $2p$ photoelectrons, respectively. The escape depths calculated for a takeoff angle of 45° are 23, 16, and 13 Å for Al $2p$, Pd $3d$, and Mn $2p$ photoelectrons, respectively. When the takeoff angle is varied from 80° to 10°, the escape depth of the Mn $2p$ photoelectrons decreases from 18 to 3 Å, thus enhancing the surface sensitivity.

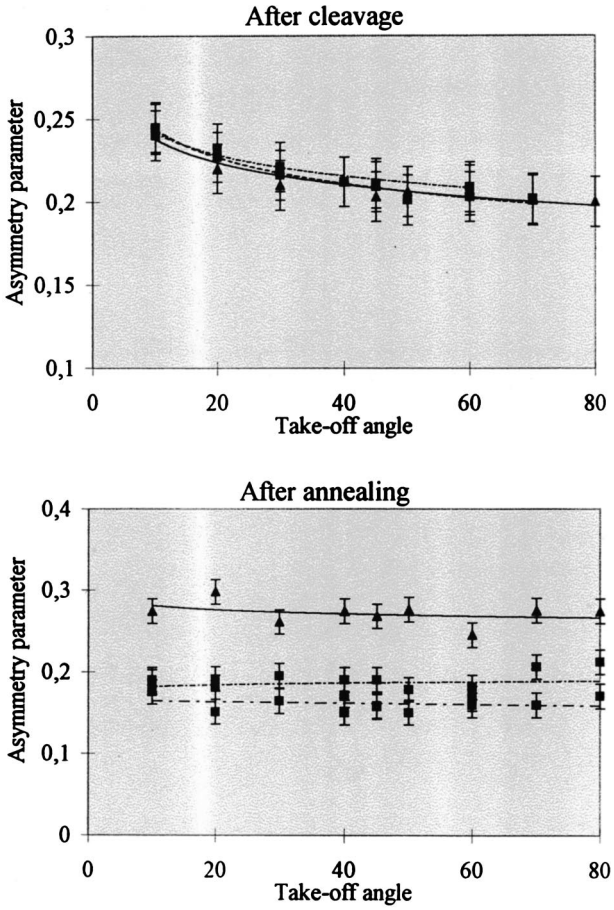

FIG. 8. Asymmetry parameter as a function of the takeoff angle, obtained from the threefold (triangles) and fivefold (squares) surface of i-Al-Pd-Mn. Amplitude of the error bars is equal to 3σ, where σ is the standard deviation.

We obtained the values of the asymmetry coefficient α from the Doniach-Sunjic fits of the Mn $2p$ core-level lines at different takeoff angles, for the fivefold and threefold surfaces of the AlPdMn quasicrystal. Experiments were conducted either for the fractured surface at room temperature or for the heat-treated surface (T above 820 K), with or without preliminary ion sputtering. The results are presented in Fig. 8. Solid lines represent a least-squares fit to the set of data obtained from each sample.

A continuous decrease of α is observed for the nascent fractured surface when the escape depth is increased [Fig. 8(a)]. This means that the asymmetry parameter for atoms nearest the surface of the quasicrystal is larger than for those deeper in the bulk, indicating a higher DOS near E_F, screening the core hole more efficiently. This enhancement of the surface density of states at the Fermi level has also been observed by Neuhold *et al.* on a fractured fivefold surface of icosahedral AlPdMn.[49] Their experiment was performed us-

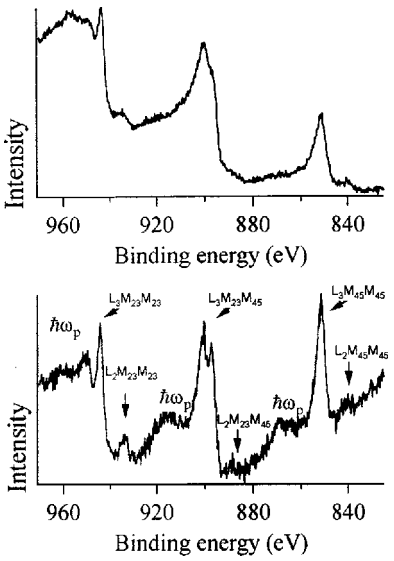

FIG. 9. Mn *LMM* Auger spectra for pure Mn (top) and for the annealed fivefold icosahedral quasicrystal (bottom).

ing synchroton radiation, which allowed them to tune the escape depth of the photoelectrons over a larger range, by varying the energy of the incoming photons. From the lineshape analysis of the Al $2p$ core levels, a higher DOS at E_F at the fractured surface was deduced, in agreement with our observation.

Once our surface has been annealed above 820 K, the asymmetry coefficient α remains constant, independent of the escape depth of the photoelectrons [Fig. 8(b)]. It does not depend on whether the surface has been previously sputtered or not. Therefore heat treatment does not enhance the surface DOS.

H. Auger line shapes

As noted first by CJJ and mentioned here on several occasions, the narrowing of the Mn $2p_{3/2}$ line is partly due to the reduction of the intrinsic linewidth 2γ. A decrease of γ means that the lifetime of the core hole increases. The decay of the core hole is dominated by Auger processes. In the case of the $2p$ hole of Mn, half of the total transition probability involves $3d$ electrons, through the $L_{23}CM_{45}$ and $L_{23}M_{45}M_{45}$ transitions.[50,51]

Figure 9 shows the *LMM* Auger spectra for the annealed fivefold surface as compared to pure Mn, measured using the same resolution. The peaks are labeled using the spectroscopic notations. The data are quite scattered in the case of the icosahedral phase, due to the weak intensity of the signal and the relatively low Mn content. We choose not to smooth the data.

The Auger spectrum is composed of the L_2MM and L_3MM groups. The intensity of the L_2MM group is very low, due to rapid $L_2L_3M_{45}$ Coster-Kronig (CK) decay processes that decrease the number of L_2 vacancies. The fast CK transition reduces the lifetime of the L_2 photohole and this accounts for the larger width of the L_2 level as compared to L_3, observed in both the Mn metal and in the quasicrystal. The difference $[2\gamma(L_2)-2\gamma(L_3)]$ is a good measure of the CK transition rate, because other contributions to $2\gamma(L_2)$ and $2\gamma(L_3)$ are almost identical.[50] Using the values reported in Table I, we find that CK transitions contribute more than 60% of the L_2 linewidth for Mn, in accordance with published data.[52] This contribution is increased to 65% in the case of the cubic alloy, and to about 75% for the threefold and fivefold quasicrystalline surfaces, as well as for the ξ'-AlPdMn and o-Al_6Mn. This suggests that the probability of CK transitions is increased in the quasicrystal relative to pure Mn. As a result, the area ratio $A(L_3M_{45}M_{45})/A(L_2M_{45}M_{45})$ should be lower in the alloy than in Mn. A rough estimate of these ratios from the experimental data gives the values 8 and 21, for the quasicrystal and for Mn, respectively.

The features noted $\hbar\omega_p$ in the figure corresponding to the quasicrystal, located at about 17 eV from the main peaks, are probably due to the excitation of plasmons, as they have the same energy as the energy-loss structure observed in the Mn $2p$ core-level spectra.

The main difference between the Auger spectra of i-AlPdMn and pure Mn is that the two components of the $L_3M_{23}M_{45}$ ($L_3M_2M_{45}$ and $L_3M_3M_{45}$) are resolved in the case of the annealed quasicrystal whereas they are not in the metal. The $L_3M_{45}M_{45}$ line is also more narrow in the annealed quasicrystal (FWHM of the peak is 4.0 eV versus 5.3 eV for pure Mn). The $L_3M_{45}M_{45}$ should reflect the self-convolution of the Mn $3d$ band and the $L_3M_{23}M_{45}$ the convolution of the $3d$ band with the $3p$ levels. The energy gap between the two components of the $L_3M_{23}M_{45}$ line does not vary and is equal to 4 eV in Mn metal as in the quasicrystal. Consequently, the splitting of the $L_3M_{23}M_{45}$ Auger line can be ascribed to the narrowing of the Mn $3d$ band in the annealed quasicrystal. We note also that the distribution of the occupied Mn $3d$ states lies very close to E_F, in the quasicrystal and in pure Mn. A narrower distribution of the Mn $3d$ states in the quasicrystal is consistent with a pseudogap at E_F.

We observed that the narrowing of the Mn $2p_{3/2}$ core-level line is due partly to the reduction of the intrinsic linewidth 2γ, i.e., to an increase of the $2p_{3/2}$ photohole lifetime in the quasicrystal. This corresponds to a decrease in the rate of filling of the photohole. Because the filling of the photohole is dominated by the Auger process, we expect the Auger transition probabilities (intensities) for filling the $2p_{3/2}$ states to be reduced. Furthermore, the Mn $3d$ states lie in the VB and are more likely to be sensitive to the chemical and structural environment than deep core levels, so we expect Auger transitions involving the Mn $3d$ states to be affected preferentially. Following this idea, we tried to estimate the intensity ratios of Auger lines involving $3d$ states, vs those which do not involve the Mn $3d$ states. These ratios are $A(L_3M_{45}M_{45})/A(L_3M_{23}M_{23})$ and $A(L_3M_{23}M_{45})/A(L_3M_{23}M_{23})$. The $L_3M_{45}M_{45}$ and $L_3M_{23}M_{45}$ are the Auger transitions contributing to the filling of the Mn $2p_{3/2}$ (L_3) hole and involving the Mn $3d$ (M_{45}) states. The $L_3M_{23}M_{23}$ was chosen as the reference because this transition implies only core levels and should stay atomic in nature. We chose to subtract a linear background below each Auger line. The ratios were about 3 and 7, respectively, for the metal, reduced to about 2 and 5 for the annealed quasicrystal. The reduction of these ratios indicates a decrease of the $3d$-containing Auger transition rates

in the quasicrystal relative to the metal. This could be due to an increased localization of the $3d$ states in the quasicrystal, that will lower the probability for a $3d$ electron to fill a $2p$ photo hole. This is consistent with the reduction of the intrinsic lifetime 2γ of the Mn $2p_{3/2}$ core level.

IV. DISCUSSION

Perhaps the most intriguing result of this work is the difference in metallic character between the fractured surfaces and the sputter-annealed surfaces. The former shows less metallic character at the very surface region, than does the latter. Two possible explanations to account for the higher DOS at the fractured surface relative to the bulk have been proposed.[49] They rely on two different descriptions of the electronic structure of quasicrystals. We will now discuss their ability to account for the interesting results presented here.

One explanation is based on usual band-structure argument and leads to a Hume-Rothery description of quasicrystals. The interaction between the Fermi sphere and a predominant pseudo-Brillouin zone (FS/PBZ interaction) results in a van Hove singularity of the DOS located at E_F, the so-called pseudogap. The pseudo-Brillouin zone is constructed from the reciprocal-lattice vectors associated with the strongest Fourier components of the pseudopotentials. Due to the high symmetry of the icosahedral point group, the pseudo-Brillouin zone is almost spherical, the matching with the Fermi sphere is optimal, and a deeper pseudogap results, lowering the band energy of the system. The presence of the Mn *d* states close to the Fermi energy, hybridized with ''normal'' *sp* states, leads to an increase of the potential diffracting the Fermi electrons, thus increasing the width of the pseudogap.[53] Following the Hume-Rothery arguments, the stability of quasicrystals is thus explained rather well. Introducing a surface by fracturing the sample will then lower the symmetry of the pseudo-Brillouin zone, decreasing the depth of the pseudogap at E_F. A higher DOS at E_F may result, consistent with what we observe for the fractured surface, at room temperature.

We must now examine if the experimental data for the heat-treated surface are consistent within this model. Surface x-ray diffraction, low-energy ion scattering (LEIS), and LEED characterization of the same fivefold surface, prepared by sputtering and annealing, showed a contraction of the outermost atomic layer and a depletion in Mn. A contraction of the characteristic interatomic distances in real space will result in an increase of the characteristic distances in reciprocal space. The radius of the predominant pseudo-Brillouin zone will then be increased. In order to maintain the Hume-Rothery stabilization, the radius of the Fermi sphere (i.e., the concentration of valence electrons) should be increased to match the pseudo-Brillouin zone. The valence of Al and Pd atoms being higher than that of Mn, a depletion of Mn in the annealed surface does effectively increase the valence electron concentration in the topmost layers. Therefore the observed chemical and structural modifications upon annealing are consistent within the Hume-Rothery framework as a necessity in order to maintain the Fermi level in the pseudogap of the DOS up to the surface, i.e., a situation which enhances the stability of the system.

For this interpretation, one must consider that Mn depletion does not appear to be unique to the quasicrystal. For all of the fracture surfaces we have studied—including the ξ' and the orthorhombic phase—XPS shows a depletion in Mn concentration during the process of annealing. We note that the decrease in Mn at the fracture surface of the icosahedral phase after annealing has been reported previously, based upon Auger electron spectroscopy.[54] The deficiency in Mn at the surface of *i*-Al-Pd-Mn prepared by sputter annealing has also been reported from earlier observations by low energy in scattering,[55] and surface x-ray diffraction.[56] Nothing is known about the structures of the topmost layers in ξ' or Al_6Mn, nor do we know whether an enhanced DOS will be observed for the fractured surfaces of these materials. Nonetheless, if Mn depletion at the surface is indicative of an electronic stabilization, we can predict a contraction of the topmost layers in these alloys too, in order to maintain the FS/BZ matching.

The second explanation is based on a totally different approach, whose starting point is the description by Janot and de Boissieu of quasicrystals as a self-similar hierarchical packing of atomic clusters.[57–59] Indeed, the fractured fivefold surface of an icosahedral AlPdMn single grain observed by STM has large corrugation (10 Å) and shows the presence of clusters 8–10 Å in diameter.[9] The clusters seem to form a self-similar hierarchical structure.[9] The quasicrystalline fivefold surface prepared by sputtering and annealing at temperatures higher than 700 K has also been investigated by STM, LEED, and x-ray scattering.[6–8,24,36,37,55,60] These experiments show a very different structure, with terraces and steps, and a terrace corrugation smaller than 1 Å. However, recent analyses of the fine structure on the terraces, observed by STM at high resolution, demonstrated that these features do not correspond to atoms but rather to clusters of atoms, separated by filler material.[60,61] Therefore the two types of surface structures may be described using the same structural building blocks, i.e., atomic clusters with fivefold symmetry (pseudo-Mackay or Bergman clusters). Published analysis of the fractured surface by STM revealed that over at least some of the surface, the cluster-subcluster structure evolves upon annealing toward a terrace-step topography.[10]

In terms of electronic structure, the clusters are treated as spherical potential wells, each containing a magic number of electrons, corresponding to the exact filling of the electronic shells of the hierarchy of wells. The DOS is described as the superposition of the bonded states of the successive hierarchy of clusters. The unbounded states of one generation are the bonded states of the next generation, and the Fermi level is located in a valley separating the unoccupied free electron states from the occupied bonded states of the hierarchy of clusters. Introducing a surface by fracturing is a perturbation of the hierarchical order and should shift the Fermi level away from the pseudogap. This would then explain the results presented above for the fractured surface. In the cluster model, interaction between aggregates depends on the distribution of the electronic states close to the Fermi level, and their geometrical arrangement should minimize this interaction energy, by creating a pseudogap at E_F. The evolution toward a terrace-step topography upon annealing (starting either from a fracture surface or from a sputtered surface) may account for the rearrangement of the cluster units in

order to minimize this interaction energy in the presence of a surface. This second model could also account for our above observations. However, the detailed mechanisms involved in such structural and chemical rearrangement remain to be elucidated.

V. SUMMARY

In summary, we have shown that the narrowing of the Mn $2p_{3/2}$ core-level line observed in *i*-Al-Pd-Mn is a direct consequence of the presence of a pseudogap at the Fermi level and should not be considered as the fingerprint of the quasicrystalline phase. This is because a narrow Mn $2p_{3/2}$ line is also observed in the ξ'-AlPdMn approximant and in the orthorhombic Al_6Mn crystal. The latter is an alloy of the Hume-Rothery type. A similar narrowing of the Fe $2p_{3/2}$ core-level line can be seen in the *i*-Al-Cu-Fe quasicrystal, reflecting a low density of states at the Fermi edge, consistent with the expectation that the electronic structure is of great importance in the stabilization of the icosahedral phases. The analysis of the photoelectron spectra of the sputtered surface as a function of the annealing temperature indicates a transition in the electronic structure, associated with a rearrangement of the local atomic order. After sputtering and annealing to temperatures below 720 K, the Mn line shows an asymmetric tail and the valence band develops a clear Fermi edge, indicating that the system is metallic with no pseudogap at the Fermi level. The electronic structure and the composition are then very similar to the cubic Al-Pd-Mn alloy. A transition occurs upon annealing at temperatures higher than 770 K: the Mn line narrows and the slope of the valence band in the region near the Fermi level is reduced, reflecting the presence of a pseudogap.

The low DOS at E_F is observed in the surface *plus* near surface region of the quasicrystal, whether the surface has been prepared by fracturing in UHV or by ion sputtering with high-temperature annealing. However, when the surface sensitivity is increased, photoelectron spectroscopy shows that the bulk pseudogap is not retained up to the nascent fractured surface, while it is retained when the same surface is annealed above 770 K, or when the surface is prepared by sputtering and annealing above 770 K. The transformation upon heat treatment is associated with variations in the composition. The above results suggest that the heat-treated surface is more stable than the surface obtained by fracturing at room temperature. The structural and chemical modifications observed upon annealing are associated with a lowering of the electronic contribution to the energy of the system. The stabilization mechanisms of the surface seem similar to those of the bulk icosahedral quasicrystal.

ACKNOWLEDGMENTS

We thank Cynthia Jenks for her generous and skilled assistance. This work was supported by the Ames Laboratory, which is operated for the U.S. Department of Energy by Iowa State University under Contract No. W-7405-Eng-82, and by Program International de Coopération Scientifique (PICS) under Grant No. 545 NSF-CNRS.

[1] D. Shechtman, I. Blech, D. Gratias, and J. W. Cahn, Phys. Rev. Lett. **53**, 1951 (1984).

[2] C. Janot, *Quasicrystals: A Primer*, edited by C. J. Humphreys, P. B. Hirsch, N. F. Mott, and R. J. Brook, Monographs on the Physics and Chemistry of Materials Vol. 48 (Clarendon Press, Oxford, 1992).

[3] S. S. Kang, J. M. Dubois, and J. von Stebut, J. Mater. Res. **8**, 2471 (1993).

[4] J.-M. Dubois, S. S. Kang, and A. Perrot, Mater. Sci. Eng., A **179/180**, 122 (1994).

[5] P. A. Thiel, C. J. Jenks, and A. I. Goldman, in *Physical Properties of Quasicrystals*, edited by Z. Stadnik (Springer-Verlag, Berlin, 1999), p. 327.

[6] T. M. Schaub, D. E. Bürgler, H.-J. Güntherodt, and J. B. Suck, Phys. Rev. Lett. **73**, 1255 (1994).

[7] T. M. Schaub, D. E. Bürgler, H.-J. Güntherodt, and J.-B. Suck, Z. Phys. B: Condens. Matter **96**, 93 (1994).

[8] T. M. Schaub, D. E. Bürgler, H.-J. Güntherodt, J. B. Suck, and M. Audier, Appl. Phys. A: Mater. Sci. Process. **61**, 491 (1995).

[9] P. Ebert, M. Feuerbacher, N. Tamura, M. Wollgarten, and K. Urban, Phys. Rev. Lett. **77**, 3827 (1996).

[10] P. Ebert, F. Kluge, B. Grushko, and K. Urban, Phys. Rev. B **60**, 874 (1999).

[11] Z. M. Stadnik, D. Purdie, M. Garnier, Y. Baer, A.-P. Tsai, A. Inoue, K. Edagawa, and S. Takeuchi, Phys. Rev. Lett. **77**, 1777 (1996).

[12] Z. M. Stadnik, D. Purdie, M. Garnier, Y. Baer, A.-P. Tsai, A. Inoue, K. Edagawa, and S. Takeuchi, Phys. Rev. B **55**, 10 938 (1997).

[13] X. Wu, S. W. Kycia, C. G. Olson, P. J. Benning, A. I. Goldman, and D. W. Lynch, Phys. Rev. Lett. **75**, 4540 (1995).

[14] D. Naumovic, P. Aebi, L. Schlapbach, C. Beeli, T. A. Lograsso, and D. W. Delaney, Phys. Rev. B **60**, R16 330 (1999).

[15] G. K. Wertheim and P. H. Citrin, in *Photoemission in Solids I*, edited by M. Cardona and L. Ley (Springer-Verlag, Berlin, 1978).

[16] G. D. Mahan, Phys. Rev. **163**, 612 (1967).

[17] J. C. W. Folmer and D. K. G. d. Boer, Solid State Commun. **38**, 1135 (1981).

[18] C. J. Jenks, S.-L. Chang, J. W. Anderegg, P. A. Thiel, and D. W. Lynch, Phys. Rev. B **54**, 6301 (1996).

[19] G. Cappello, A. Dechelette, F. Schmithüsen, J. Chevrier, F. Comin, A. Stierle, V. Formoso, M. de Boissieu, T. Lograsso, C. Jenks, and D. Delaney, in *Quasicrystals*, edited by J. M. Dubois, P. A. Thiel, A. P. Tsai, and K. Urban, MRS Symposia Proceedings No. 553 (Materials Research Society, Warrendale, PA, 1999), pp. 243–249.

[20] Z. Shen, M. J. Kramer, C. J. Jenks, A. I. Goldman, T. Lograsso, D. Delaney, M. Heinzig, W. Raberg, and P. A. Thiel, Phys. Rev. B **58**, 9961 (1998).

[21] B. Bolliger, M. Erbudak, D. D. Vvedensky, M. Zurkirch, and A. R. Kortan, Phys. Rev. Lett. **80**, 5369 (1998).

[22] See Reference 19, pp. 257–262.

[23] F. Shi, Z. Shen, D. W. Delaney, A. I. Goldman, C. J. Jenks, M. J.

Kramer, T. Lograsso, P. A. Thiel, and M. A. V. Hove, Surf. Sci. **411**, 86 (1998).
[24] Z. Shen, W. Raberg, M. Heinzig, C. J. Jenks, M. Gierer, M. A. V. Hove, T. Lograsso, T. Cai, and P. A. Thiel, Surf. Sci. (to be published).
[25] D. W. Delaney, T. E. Bloomer, and T. A. Lograsso, *Suppression of Secondary Phases during Growth of Icosahedral A170Pd21.5Mn8.5*, edited by A. I. Goldman, D. Sordelet, P. A. Thiel, and J. M. Dubois, New Horizons in Quasicrystals: Research and Applications (World Scientific, Ames, IA, 1996).
[26] T. A. Lograsso and D. W. Delaney, J. Mater. Res. **11**, 2125 (1996).
[27] T. A. Lograsso and D. W. Delaney, in *Proceedings of the Sixth International Conference on Quasicrystals (ICQ6)*, edited by S. Takeuchi and T. Fujiwara (World Scientific, Singapore, 1998), pp. 325–328.
[28] C. J. Jenks, P. J. Pinhero, Z. Shen, T. A. Lograsso, D. W. Delaney, T. E. Bloomer, S.-L. Chang, C.-M. Zhang, J. W. Anderegg, A. H. M. Z. Islam, A. I. Goldman, and P. A. Thiel, in *Proceedings of the 6th International Conference on Quasicrystals (ICQ6)* (Ref. 27), pp. 741–748.
[29] M. Boudard, H. Klein, M. D. Boissieu, M. Audier, and H. Vincent, Philos. Mag. A **74**, 939 (1996).
[30] P. Canfield and Z. Fisk, Philos. Mag. B **65**, 1117 (1992).
[31] I. R. Fisher, M. J. Kramer, Z. Islam, T. A. Wiener, A. Kracher, A. R. Ross, T. A. Lograsso, A. I. Goldman, and P. C. Canfield (unpublished).
[32] A. Kontio and P. Coppens, Acta Crystallogr., Sect. B: Struct. Crystallogr. Cryst. Chem. **37**, 433 (1981).
[33] S. Doniach and M. Sunjic, J. Phys. C **3**, 285 (1970).
[34] G. K. Wertheim and L. R. Walker, J. Phys. F **6**, 2297 (1976).
[35] G. K. Wertheim and S. B. Dicenzo, J. Electron Spectrosc. Relat. Phenom. **37**, 57 (1985).
[36] T. M. Schaub, D. E. Bürgler, H.-J. Güntherodt, J. B. Suck, and M. Audier, in *Proceedings of the 5th International Conference on Quasicrystals (ICQ5)*, edited by C. Janot, and R. Mosseri (World Scientific, Singapore, 1995), pp. 132–138.
[37] M. Gierer, M. A. V. Hove, A. I. Goldman, Z. Shen, S.-L. Chang, C. J. Jenks, C.-M. Zhang, and P. A. Thiel, Phys. Rev. Lett. **78**, 467 (1997).
[38] E. Belin, Z. Dankházi, A. Sadoc, and J. M. Dubois, J. Phys.: Condens. Matter **6**, 8771 (1994).
[39] Z. Shen, P. J. Pinhero, T. A. Lograsso, D. W. Delaney, C. J. Jenks, and P. A. Thiel, Surf. Sci. **385**, L923 (1997).
[40] Z. Shen, C. J. Jenks, J. Anderegg, D. W. Delaney, T. A. Lograsso, P. A. Thiel, and A. I. Goldman, Phys. Rev. Lett. **78**, 1050 (1997).
[41] F. U. Hillebrecht, J. C. Fuggle, P. Bennet, Z. Zolnierek, and C. Freiburg, Phys. Rev. B **27**, 2179 (1983).
[42] A. P. Smith and N. W. Ashcroft, Phys. Rev. Lett. **89**, 1365 (1987).
[43] D. Mayou, C. Berger, F. Cyrot-Lackmann, T. Klein, and P. Lanco, Phys. Rev. Lett. **70**, 3915 (1993).
[44] T. Takeuchi and U. Mizutani, Phys. Rev. B **52**, 9300 (1995).
[45] G. T. de Laissardière, D. Mayou, and D. N. Manh, Europhys. Lett. **21**, 25 (1993).
[46] T. Grenet, C. Berger, and M. C. Cheynet, in *Proceedings of the Sixth International Conference on Quasicrystals (ICQ6)* (Ref. 27), p. 599.
[47] C. J. Powell, A. Jablonski, I. S. Tilinin, S. Tanuma, and D. R. Penn, J. Electron Spectrosc. Relat. Phenom. **98–99**, 1 (1999).
[48] M. Boudard, M. de Boissieu, C. Janot, G. Heger, C. Beeli, H.-U. Nissen, H. Vincent, R. Ibberson, M. Audier, and J. M. Dubois, J. Phys.: Condens. Matter **4**, 10 149 (1992).
[49] G. Neuhold, S. R. Barman, K. Horn, W. Theis, P. Ebert, and K. Urban, Phys. Rev. B **58**, 734 (1998).
[50] E. J. McGuire, Phys. Rev. A **3**, 1801 (1971).
[51] J. Väyrynen, J. Electron Spectrosc. Relat. Phenom. **22**, 27 (1981).
[52] J. C. Fuggle and S. F. Alvarado, Phys. Rev. A **22**, 1615 (1980).
[53] G. Trambly de Laissardière, D. Nguyen Manh, L. Magaud, J. P. Julien, F. Cyrot-Lackmann, and D. Mayou, Phys. Rev. B **52**, 7920 (1995).
[54] P. Ebert, F. Kluge, B. Grushko, and K. Urban (unpublished).
[55] M. Gierer, M. A. V. Hove, A. I. Goldman, Z. Shen, S.-L. Chang, P. J. Pinhero, C. J. Jenks, J. W. Anderegg, C.-M. Zhang, and P. A. Thiel, Phys. Rev. B **57**, 7628 (1998).
[56] M. J. Capitan, J. Alvarez, J. L. Joulaud, and Y. Calvayrac, Surf. Sci. **423**, L251 (1999).
[57] C. Janot and M. de Boissieu, Phys. Rev. Lett. **72**, 1674 (1994).
[58] C. Janot and J.-M. Dubois, in *An Introduction to Structure, Physical Properties and Application of Quasicrystalline Alloys*, edited by J.-B Suck, M. Schreiber, and P. Hausler (Springer-Verlag, Berlin, in press).
[59] C. Janot, J. Phys.: Condens. Matter **9**, 1493 (1997).
[60] Z. Shen, C. Stoldt, C. Jenks, T. Lograsso, and P. A. Thiel, Phys. Rev. B **60**, 14 688 (1999).
[61] G. Kasner, Z. Papadopolos, P. Kramer, and D. E. Bürgler, Phys. Rev. B **60**, 3899 (1999).